

REVIEW ARTICLE

3D printable conductive composite inks for the fabrication of biocompatible electrodes in tissue engineering application

Jihwan Kim¹, Jinah Jang^{1,2,3,4*}

¹Department of Mechanical Engineering, Pohang University of Science and Technology (POSTECH), Pohang, South Korea

²Department of Convergence IT Engineering, Pohang University of Science and Technology (POSTECH), Pohang, South Korea

³School of Interdisciplinary Bioscience and Bioengineering, Pohang University of Science and Technology (POSTECH), Pohang, South Korea

⁴Institute for Convergence Research and Education in Advanced Technology, Yonsei University, Seoul, South Korea

(This article belongs to the *Special Issue: Composite/Multi-component Biomaterial Inks and Bioinks*)

Abstract

Native tissues are affected by the microenvironment surrounding the tissue, including electrical activities. External electrical stimulation, which is used in replicating electrical activities and regulating cell behavior, is mainly applied in neural and cardiac tissues due to their electrophysiological properties. The *in vitro* cell culture platform with electrodes provides precise control of the stimulation property and eases the observation of the effects on the cells. The frequently used electrodes are metal or carbon rods, but their risk of damaging tissue and their mechanical properties that are largely different from those of native tissues hinder further applications. Biocompatible polymer reinforced with conductive fillers emerges as a potential solution to fabricate the complex structure of the platform and electrode. Conductive polymer can be used as an ink in the extrusion-based printing method, thus enabling the fabrication of volumetric structures. The filler simultaneously alters the electrical and rheological properties of the ink; therefore, the amount of additional compound should be precisely determined regarding printability and conductivity. This review provides an overview on the rheology and conductivity change relative to the concentration of conductive fillers and the applications of printed electrodes. Next, we discuss the future potential use of a cell culture platform with electrodes from *in vitro* and *in vivo* perspectives.

Keywords: Extrusion-based printing; Conductive filler; Tissue engineering; Rheology; Conductivity

1. Introduction

Tissue engineering has expanded human knowledge and the ability to regenerate and reconstruct human organs. In addition, advancements in tissue engineering have enabled the fabrication of tissues that mimic the original tissue function in the *in vitro* analysis and the transplantation of engineered tissues. Recent studies have

***Corresponding author:**

Jinah Jang
(jinahjang@postech.ac.kr)

Citation: Kim J, Jang J., 2023, 3D printable conductive composite inks for the fabrication of biocompatible electrodes in tissue engineering application, *Int J Bioprint*, 9(1): 643. <https://doi.org/10.18063/ijb.v9i1.643>

Received: May 31, 2022

Accepted: July 10, 2022

Published Online: November 16, 2022

Copyright: © 2022 Author(s). This is an Open Access article distributed under the terms of the Creative Commons Attribution License, permitting distribution, and reproduction in any medium, provided the original work is properly cited.

Publisher's Note: Whioce Publishing remains neutral with regard to jurisdictional claims in published maps and institutional affiliations.

suggested that recapitulating the physical and chemical microenvironment of the tissue enhances the performance of the engineered tissues^[1]. The Electrophysiology of tissue has caught attention as an important property,^[2,3] because the tissue functions are regulated by their own or innervated nerve's electrical activities. External electrical stimulation induces the depolarization of the cell membrane, and the modification of the intracellular dynamics and ion concentration. Intracellular activities contribute to changes in the morphology of cells and the secretion of proteins or hormones, which affect cell behaviors, such as migration^[4], proliferation^[5-7], differentiation^[8], and maturation^[9-11]. The *in vitro* cell culture platform integrated with electrodes has emerged as a promising approach to exert electrical stimulation and has been shown to demonstrate meaningful results; however, the exact mechanisms of each cell function modulation have yet to be delineated. In addition, the electrical stimulation properties used in *in vitro* culture platform should be optimized. Direct current and alternating current influence cells with different mechanisms, and the voltage, current, frequency, pulse width, and duration affect the viability and behaviors of the cell^[12]. Therefore, controlled microenvironment and optimized electrical stimulation properties have always been an essential goal for the optimization of stimuli and precise analysis.

In general, *in vitro* cell culture platforms for electrical stimulation comprise two electrodes, which are placed into the aqueous media, as shown in Figure 1A. The external stimulator applies a constant voltage or current to the electrodes, while the tissue is cultured between the electrodes, where the electrical field is exerted. The electrodes are frequently composed of biocompatible metals (e.g., platinum^[11,13,14] or titanium^[15]) or carbon rods^[12]. However, metal electrodes have a risk of irreversible faradaic reactions due to their low charge injection capacity^[16,17], while carbon rods might rupture, generating harmful carbon particles due to their brittleness. In addition, the high mechanical properties and brittleness of the metal and carbon electrodes have been vital drawbacks for various applications with different sizes and designs. To address the current challenges in developing advanced electrical stimulation systems with high versatility, three-dimensional (3D) printing technology is exploited as the standard fabrication method with high spatial resolution that can apply various inks^[18].

Composite ink provides high flexibility in achieving various needs as ink for extrusion-based printing. The incorporation of insoluble fillers (e.g., nanoparticles, nanotubes, and fibers) into the composite ink affects the printability, mechanical and structural properties, and conductivity^[19]. Among various

types of composite inks, conductive ink fabricated by blending conductive fillers into biocompatible polymers has been proposed as a novel material for biocompatible electrodes. The high capacitance and elasticity potentiate the conductive ink as a safe electrode material with a low risk of damage to the electrode and tissue^[20-22]. The conductive fillers not only affect the conductivity of the polymers but also their rheological properties and printability. In general, a high concentration of fillers results in high conductivity, instead of low printability due to high viscosity and clogging of the nozzle. As high conductivity is preferable to reduce the effect of leakage current, determining an appropriate concentration of fillers is essential to achieve the best conductivity and printability. However, the nonlinear characteristic of conductivity and their relationship with the filler morphology makes predicting the optimum concentration of fillers difficult.

Increasingly, many studies on 3D volumetric tissue structures have been published, and 3D volumetric structures are known to be able to better replicate the tissue microenvironment compared to 2D structures^[23,24]. Commonly used platforms could not exert even electrical stimulation to 3D structures, thus lowering the reproducibility and consistency of the results. 3D printing with conductive ink facilitates the adjustment of printed features with electrode size, shape, number, and chamber size and shape. The assembly of bioink and conductive ink is assisted by multi-material 3D printing, which can simultaneously construct intricate structures with multiple nozzles and inks^[25]. Therefore, ink with conductive fillers play a critical role in 3D printing due to its high conductivity, printability, and biocompatibility with variable rheological properties.

First, this review discusses the mechanism of the rheology and conductivity change with the introduction of the filler. Next, we summarize some applications of conductive ink with different fillers, such as metals, carbon-based materials, and MXene. Lastly, this review examines the current state and proposes future directions on electrode integrated tissue culturing platforms fabricated ion using conductive ink for electrical stimulation or sensing of engineered tissue.

2. Basic properties of ink with fillers for the extrusion-based printing process

2.1. Understanding rheological properties as criteria of the extrusion process

The extrusion-based printing process requires precise manipulation of printing parameters (e.g., nozzle size, pressure, and feed rate) for high accuracy and reproducibility^[26]. The decision of parameters largely depends on the rheological property of the ink. Furthermore, the rheological property of the ink

contributes to alleviating clogging during printing and shape fidelity after printing.

The ink experiences high shear stress during the printing process and there is no shear stress after printing. The ink's behavior can be analyzed in terms of the resistance to deformation depending on shear stress, called viscosity,

derived from Newton's law of viscosity, $\tau = \left(\mu \frac{\partial u}{\partial y} \right)$ [27].

Materials that have a constant viscosity μ independent of the shear stress are called Newtonian materials, while materials in which the viscosity differ in accordance with the shear stress are called non-Newtonian materials [28]. The viscosity of a shear-thickening material increases with shear stress, while the viscosity of a shear-thinning material decreases with shear stress [29] (Figure 1B). Shear-thinning materials have a prominent advantage in extrusion-based printing as the shear stress during the extrusion process decreases the viscosity, facilitating its flow out from the nozzle. After extrusion, the material recovers its viscosity, resulting in high fidelity in the printed result.

Similarly, the complex modulus quantifies the viscoelastic behavior, which describes both the viscous and elastic behaviors under deformation [29]. Complex modulus comprises the storage (G') and loss modulus (G'') [30]. The storage modulus measures the stored energy, which represents the material's elastic behavior, while the loss modulus measures the energy dissipated through heat, which represents the material's viscous behavior. The $\tan \delta$ value is defined as the ratio of the loss modulus over storage modulus (G''/G'), which indicates whether a material is elastic ($\tan \delta < 1$) or viscous ($\tan \delta > 1$) [30]. The modulus varies with conditions such as the shear stress or temperature. The complex modulus shows the behavior of the material concerning the shear stress and time. Thixotropy represents the rheological property, in which the viscosity of a material recovers over time [31]. Figure 1C shows the common complex modulus of a thixotropic material with respect to time, and Figure 1D shows the $\tan \delta$ value with applied shear stress. The thixotropic behavior affects the hardening of the ink after printing and increases the printing fidelity.

2.2. Understanding the property of a filler and the forces between fillers

Biocompatible polymers are frequently used as the base material for bioelectronic devices. To meet the myriad properties of natural tissue, the properties of polymers are modified by adding fillers (Figure 2A). The introduced fillers can upregulate the mechanical properties and provide electrical conductivity. Fillers with high conductivity have

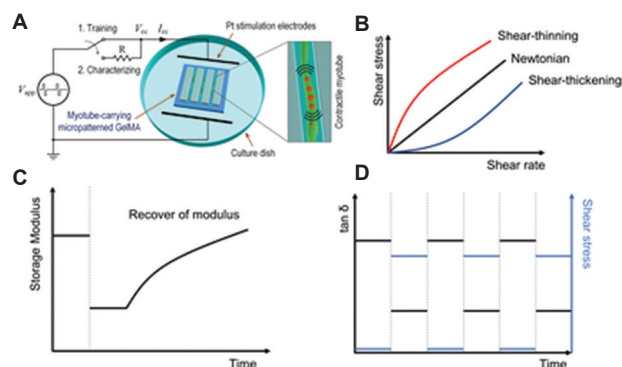


Figure 1. (A) Typical design of an electrical stimulation system with metal rod, (A) reproduced from Ref. [11] under Creative Commons License, (B) Three types of fluids in terms of viscosity, (C and D) Commonly examined rheological properties with respect to time.

diverse sizes and aspect ratios, ranging from nanometer scales to micrometer scales, spherical to rods or platelets. The aspect ratio is the largest characteristic length divided by the opposite length; the aspect ratio of a cylinder is defined as L/D and that of a platelet is defined as D/L (Figure 2B). The distance between particles, which depends on the concentration of the filler greatly affects the properties of an ink. The interparticle distance (denoted as H in Figure 2B) typically has a value of several nanometers for an ink with a high concentration filler.

The properties of the ink rely on the interactive forces between particles or between particles and the ink [32]. The colloidal interactions are the dominant force when the concentration is high and the particles are sufficiently close. The Van der Waals force acts as an attractive force between particles [33] that are closer to several nanometers. A high aspect ratio ($>1,000$) [34] and low particle size contribute to an increase in the contact site and the Van der Waals force [32]. The attractive depletion force develops when the filler is large and dispersed in the ink with non-adsorbing small molecules [35]. The electrostatic force is a repulsive force when the fillers have a charge [33] and the behavior of fillers is determined by the correlation between three forces (Figure 2C).

3. Properties of ink with conductive fillers for extrusion-based printing process

3.1. Modifying rheological and electrical properties with filler supplement

The addition of fillers modifies the ink's rheological properties. The attractive force between particles constructs a 3D structural linkage within the ink and upregulates the ink's viscosity with the filler at low shear stress. When shear stress is applied, the bond between particles "slips" to another particle [36]. This "slip" modifies

the distance between particles and breaks down the linkage, leading to low viscosity. In addition, viscous interactions, which represent the friction between particles and the surrounding matrix, overwhelm the colloidal interactions. Fillers with a high aspect ratio have a larger surface area, which results in high friction and viscosity compared to the fillers with a low aspect ratio^[37]. After printing, the particles reform their bonds and retain their viscosity. The alteration of the rheological property enhances the shear-thinning behavior of the material and yields high printability and fidelity in the printed product^[38].

The conductivity of the ink increases proportionally with the concentration of the conductive fillers. High conductivity contributes to low-energy dissipation and reduces the leakage current and tissue damage^[22]. Electrons and ions move with an electrical field, causing an electrical conduction in conductive ink. The conductivity of metals or carbon originates from mobile electrons, which is known as electronic conductivity. When electrolytes are included in the material, the charges can be transferred through ions, which is known as ionic conductivity^[39]. The electronic conductivity originates from the network formed by the conductive fillers with the interactive forces. In a high concentration of filler, direct contact between fillers works as a conductive path^[40]. However, it is known that direct contact is not the main root of conductivity. Meanwhile, in the part, where fillers do not directly contact with each other, electrons pass through the polymer by the quantum tunneling effect, hopping over the non-conductive polymer^[41]. The main charge transport mechanism is known to be electron tunneling in a percolated network^[42]. Percolation theory implies that the rigid network of the conductive path is formed over percolation threshold concentration. The conductivity is calculated using the empirical equation^[43];

$$\sigma = \sigma_0 (V - V_c)^t$$

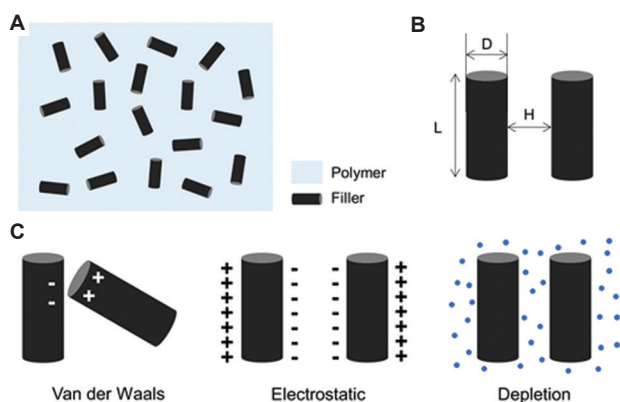


Figure 2. (A) Conductive fillers are blended in polymer. Properties of fillers (B) and forces between fillers (C).

Where σ is the conductivity of the ink, V is the volume fraction of filler, V_c is the volume fraction of filler at the percolation threshold, and σ_0 and t values are determined analytically. The equation is only valid when the concentration is greater than the percolation threshold concentration. **Figure 3** shows a typical conductivity increase of ink with conductive filler. The conductivity rapidly increases around the percolation threshold and saturates beyond that. Therefore, the percolation threshold is an important criterion in the selection of filler and their concentrations.

The rheology and conductivity of the ink differ greatly in proportion with concentration, particle size^[44], and aspect ratio^[34] of the filler. For example, when using a filler with a high aspect ratio, the percolation threshold will be low due to the large contact surface. The ink will show low printability due to the highly attractive forces between the fillers. Therefore, a relatively low concentration of filler should be chosen for the ink to be easily extruded, with conductivity reaching the saturation value (over the percolation threshold). In addition, a high concentration of fillers is known to decrease cell viability^[45]. Hence, one should decide the required conductivity of the bioelectronic device and the printing process and then choose the appropriate filler and ink concentration considering the cell viability.

3.2. Various methods for preparing conductive ink

The printability and reproducibility depend not only on the property and concentration of the filler but also on the ink's dispersion state. Uneven dispersion of the ink leads to nozzle clogging and low-quality printing results. The fillers inside the polymer tend to aggregate due to the interactive forces between particles^[46]. This aggregation increases the minimum distance between the agglomerate, thus increasing the percolation threshold concentration and lowering the conductivity of the ink at the same concentration^[47,48]. In addition, Brownian interactions

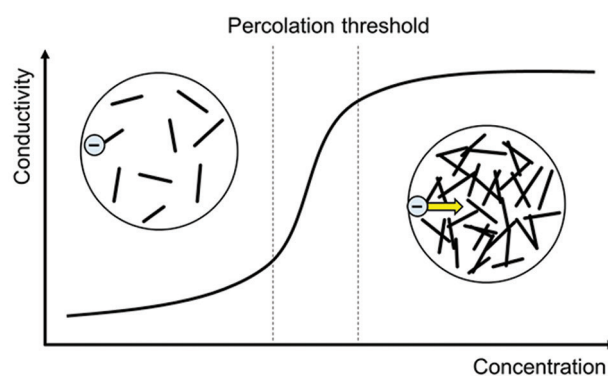


Figure 3. The conductivity increases with concentration.

dominate the behavior of inks with low concentration and low viscosity^[33], and if gravitational forces exceed the Brownian forces, the fillers will sediment during the procedure. This section describes the commonly used methods to achieve an even distribution of fillers.

3.2.1. Physical method

The simple way to mix filler with polymer is through mechanical mixing with a stirrer. A solvent is usually added to the polymer and filler, as the composite usually has high viscosity during the stirring process. Although a large, low-aspect-ratio filler can be dispersed evenly inside a polymer via mechanical mixing, fillers with a high aspect ratio, such as carbon nanotubes (CNTs), showed piles of agglomerates even after the mixing process ended and tended to reaggregate^[49]. Fillers with a high aspect ratio tend to have higher interactive forces due to the high surface area as discussed before. Energy higher than the interactive forces should be transmitted to break down the agglomerate. The sonication method applies ultrasound waves through the composite and exfoliates the agglomerates. However, extensive or long exposure to sonication may cause fracturing of the filler, diminishing the mechanical and electrical properties^[32]. In addition, increases in temperature may affect the material's properties. Therefore, the sonication power and the on/off interval should be adjusted specifically for the filler.

3.2.2. Chemical method

The difference in the polarity of the filler and the polymer hinders the blending of the filler and enhances the reaggregation tendency during the curing process. Adding surfactant considering the chemical bond with the base polymer and the composites helps even out the distribution, leading to high printability and conductivity. Gold nanorods (GNRs) tend to aggregate due to the attractive interactions between particles. Cetyltrimethylammonium bromide (CTAB) is a commonly used surfactant, although it exhibits toxicity to cells and tissues. Zhu *et al.* coated gelatin methacryloyl (GelMA) on a CTAB bilayer to fabricate GelMA-coated GNRs (G-GNRs)^[50]. The conductive ink produced by mixing G-GNR filler with an alginate prepolymer solution showed cytocompatibility and enhanced electrical signal transmission between cardiac cells. Likewise, CNT also showed a tendency to aggregate due to the Van der Waals force^[51]. Surfactants such as sodium dodecyl sulfate can be used to achieve better dispersion^[52]. Similarly, surface modification through chemical functionalization plays a crucial role in steady dispersion^[53]. Ravanbakhsh *et al.* dispersed multiwalled carboxylic (-COOH) functionalized CNTs

with triton X-100 as a surfactant to prevent the generation of agglomerates^[54].

4. Various types of conductive fillers and applications in extrusion-based printing

4.1. Metal fillers

Metal nanomaterials show high conductivity and are used as conductive filler. Gold and silver nanoparticles (AgNPs) have been commonly used to create flexible electronics, and their use has been expanded for bioelectronics. However, their high cost and the high-temperature sintering process^[55] have been main drawbacks for their implementation in the 3D printing platforms. Recently, zinc (Zn) has been adapted as a novel electrode material on the basis of its sufficient levels of biodegradability and biocompatibility^[56]. The biocompatibility of polymers, concentration of filler, conductivity and rheological properties, synthesis method, and the application of each type of filler are discussed below (Table 1).

4.1.1. Silver-based printing ink

Silver has high electrical conductivity and stability in water and is used for diagnostic and therapeutic purposes. Ahn *et al.* dispersed AgNPs with mean size of 20 nm into poly(acrylic acid) by sonication process^[57]. The conductivity of the 70 wt% ink was 10⁷ S/m after annealing for 30 min at 250°C, almost reaching the conductivity of bulk silver (10⁸ S/m). The elastic modulus of the ink increased from 10 Pa to 10⁴ Pa with a concentration of the filler from 60 wt% to 75 wt% and a viscosity as around 10–100 Pa·s. A high elastic modulus enabled the printing of the structure of several layers with high fidelity. Furthermore, the structure can be built vertically at any angle (e.g., overhanging electrode).

Britton *et al.* used silver nanowires (AgNW) as a filler in the base polymer ω -pentadecalactone-co- ϵ -decalactone copolymer (PDL)^[58]. AgNW has a high aspect ratio with an average diameter of 30 nm, an average length of 100–200 μ m. Due to the high aspect ratio, the PDL/AgNW ink showed a low percolation threshold concentration of 0.4 wt% and high storage modulus of >10⁵ Pa at 2 wt%. The sheet resistance of the ink was around 320 Ω /sq. The strain gauge of PDL/AgNW ink was printed and embedded in pristine PDL film, and the biocompatibility study showed the reduction of astrocyte area, which is activated by the foreign body reaction.

4.1.2. Zn-based printing ink

Zn is a biodegradable and biocompatible material used for biomedical applications. Farizhandi *et al.* blended Zn particles (<44 μ m) in poly(glycerol-co-sebacate) acrylate (PGSA) and chemically sintered Zn particles with acetic

Table 1. Type of conductive fillers and the properties of ink

	Filler	Polymer	Concentration	Method	Conductivity	Application	Ref.
Metal	Silver nanoparticles	Poly(acrylic acid)	70 wt%	Sonication	107 S/m	Self-supporting microelectrodes	[57]
	Silver nanowires	ω -pentadecalactone-co- ϵ -decalactone copolymer	2 wt%	–	320 Ω /sq	Strain biosensor	[58]
	Gold nanoparticle	GelMA	0.1 mg/ml	–	0.82 \pm 0.07 S/m	Conductive scaffold	[67]
	Zinc particles (<44 μ m)	poly(glycerol-co-sebacate) acrylate	70%	Chemical sintering	1.6886 \pm 0.4310 S/m	Conductive ink	[59]
Carbon	MWCNT	Gellan Gum	>30 wt%	Sonication	5030 S/m	Strain gauge	[52]
	SWCNT	GelMA	37.5 wt%	DNA surfactant sonication	128 \pm 15 S/cm	Strain gauge 3D conductive construct	[68]
	SWCNT	Cellulose nanofibrils/alginate	20 wt%	Pluronic F-127 surfactant sonication	213.2 S/m	Conductive scaffold	[69]
	Graphene flake	Poly(lactic-co-glycolide)	75 wt%	Sonication	800 S/m	Conductive ink	[64]
	Graphene oxide	Polyvinyl alcohol	7 mg/ml	–	100 S/m	Conductive ink	[65]
	Reduced graphene oxide	Agarose	1.5 mg/ml	Thermal annealing	2.07 S/m	Bioelectrodes Strain sensors	[70]
	Electrochemically derived graphene oxide	PDMS submicrobeads	0.83 vol%	–	0.06 S/m	Wearable tactile sensors	[66]
	Graphite	PDMS	45 wt%	–	~30 S/m	Heart patches with built-in electronics	[71]
	Carbon black	Thermoplastic polyurethane	25 wt%	–	84.1 S/m	Strain gauge for cardiomyocyte	[72]
	Mxene	Metal carbide (Ti ₃ C ₂ T _x)	GelMA	0.1 mg/ml	–	0.94 S/m	Conductive scaffold
Metal carbide (Ti ₃ C ₂ T _x)		Superabsorbent polymer beads	290 mg/ml	Mechanically stirring	–	Micro-supercapacitors	[73]

GelMA: Gelatin methacryloyl, PDMS: Polydimethylsiloxane, SCNT: Single-walled carbon nanotubes, MCNT: Multi-walled carbon nanotubes

acid^[59]. The PGSA/Zn ink did not show high conductivity ($\leq 10^{-2}$ S/m) even at the high concentration ratio of 70%. The SEM image showed low network formation between Zn particles. After chemical sintering, the conductivity of PGSA/Zn ink drastically increased to >1.5 S/m for a concentration ratio of >60%. The chemical sintering formed a physical network between Zn particles, leading to high conductivity and low percolation threshold concentration. The average viscosities of PGSA/Zn ink of 50%, 60%, and 70% concentration are 52.62 Pa·s, 73.36 Pa·s, and 139.90 Pa·s, respectively, which makes extrusion difficult. After the chemical sintering process, the average viscosities dropped to 23.68 Pa·s, 27.87 Pa·s, and 35.59 Pa·s, respectively. The reduction of viscosity may be due to the agglomeration of the Zn particles, decreasing the interactive force between particles. The PGSA/Zn ink showed biocompatibility *in vitro* and *in vivo*, and degraded rapidly on the 1st day, but slowly afterward due to the hydrophobicity of PGSA.

These properties show the potential of the fabrication of implantable flexible electronic devices.

4.2. Carbon-based composite

4.2.1. CNT-based printing ink

CNT is a promising conductive filler with high conductivity and a high aspect ratio. According to the orientation of the hexagonal structure, CNTs have three different structures, namely, armchair, zigzag, and chiral^[60]. The armchair structure shows high conductivity, while the zigzag and chiral structures show semi-conductive behavior. Simulation result has indicated that the composite with armchair CNTs showed a conductivity of six orders of magnitude, which is higher than that of the composite with zigzag-type CNTs^[61]. CNT can also be divided into single- (SWCNT) and multi-walled CNT (MWCNT), which differ in terms of the diameter of the structure. The structural difference contributes to a difference in the required energy for the

distribution and percolation threshold concentration. Pidcock *et al.* dispersed MWCNT into gellan gum (GG)^[52], which is a linear, anionic polysaccharide and has been approved by both the US Food and Drug Administration and the European Union for medical usage^[62]. The biocompatible property of GG allows the use of wearable or transplantable strain gauges. The research team dispersed the ink at the ratio of 1:10-1-5:10-1 (indicating 1 mg/mL of MWNT and 0.1-0.5 mg/mL of GG) and 2:10-1-2:10-15 (indicating 1-15 mg/mL of MWNT and one-fifth of GG) with ultrasonication and analyzed the viscosity and the conductivity. The viscosity of 2:10-1 is comparable to that of water (~1 mPa·s) at all shear rates. The viscosity of 2:10-15 at a low shear rate is 1000 mPa·s, which is more than twice higher than that of 4 mg/mL GG. However, the viscosity decreases to around 200 mPa·s at a high shear rate, similar to that of 4 mg/mL GG. This observation supports the enhancement of shear-thinning behavior with the introduction of filler. The strain gauge with a gauge factor value of around 15 can be fabricated using the ink.

Pedrotty *et al.* mixed SWCNTs in nanofibrillated cellulose with the surfactant Pluronic F127 at a concentration of 1.9 wt%^[63]. The complex modulus NFC/SWCNT ink implied elastic behavior ($\tan \delta < 1$) below 100 Pa and viscous behavior ($\tan \delta > 1$) over 100 Pa, proving shear-thinning behavior for extrusion-based printing. The decrease in viscosity in response to the shear rate verifies this property. The conductivity of the NFC/SWCNT was around 43 S/m. The NFC/SWCNT ink is printed on biocompatible BNC film and attached to the ventricle incision; the conductive patch proved the ability to restore the conductive velocity of the heart.

4.2.2. Graphene-based printing ink

Graphene is a single layer of carbon sheet with high conductivity and mechanical properties. Jakus *et al.* fabricated a 3D printable graphene (3DG) composite by combining 75 wt% graphene flakes with biocompatible and biodegradable polylactide-co-glycolide (PLG)^[64]. The solvent was evaporated in a sonicating bath until the viscosity reached 30 Pa·s. The 3DG showed high fidelity that could stack >700 hundred layers and conductivity of >800 S/m after annealing. However, the hydrophobic property of graphene hinders its biomedical and implantation applications. Therefore, graphene oxide (GO), oxidized graphene that includes oxygen functional groups, or reduced graphene oxide (rGO), which is redoxed GO for its desired properties is used instead. García-Tuñón *et al.* generated a water-based paste with GO and various materials (e.g., polymers, ceramics, and steel)^[65]. GO suspension showed shear-thinning behavior when diluted in water at 0.1 - 0.6 vol%. The storage modulus

rapidly increased with the GO concentration >2 vol% to the printable range and showed shear-thinning behavior. The research team hypothesized that some GO flakes roll up at high concentrations, enhancing their elastic properties by forming strong network. The GO ink showed conductivity of around 100 S/m with and without additional components such as F127. Similarly, Shi *et al.* formulated aqueous ink with electrochemically derived GO (EGO) and polydimethylsiloxane (PDMS) submicrobeads^[66]. The PDMS/EGO ink showed shear-thinning behavior, proven by viscosity decrease with shear rate, and complex modulus. Due to its thixotropic and viscoelastic properties, ink can be printed with a small inner nozzle diameter (50 μm). After the annealing process, EGO deoxygenated and covered the PDMS submicrobeads, increasing the conductivity (0.06 S/m for 0.83 vol%).

4.3. MXene-based printing ink

After the introduction of graphene, the potential of 2D materials has caught the attention of research community. A novel 2D material called MXene is fabricated from the MAX phase, composed of Mn+1AX_n , where M is a transition metal, A is an A group (mostly IIIA and IVA group) element, X is C and/or N, and $n = 1, 2, 3$ ^[74]. The A layer can be etched out using an acid such as hydrofluoric acid, leaving the Mn+1X_n layer. MXenes show extraordinary mechanical and electrical properties. Among various types of MXenes, $\text{Ti}_3\text{C}_2\text{Tx}$, where Tx represents the surface terminators (e.g. OH, O_2 , or F), is known to be non-toxic^[75]. Boularaoui *et al.* used low-concentration GelMA hydrogels as a polymer, and $\text{Ti}_3\text{C}_2\text{Tx}$ MXene as a filler to create a conductive composite^[67]. The ink containing 0.05 mg/mL MXene showed high cell viability after day 7, although the cell viability of 0.1 mg/mL MXene dropped on day 7. The ink showed shear-thinning behavior with a slight increase in viscosity at a low shear rate as expected. The conductivity of the ink was around 0.65 S/m and 0.94 S/m at 0.05 mg/mL and 0.1 mg/mL, respectively, which is comparable to the conductivity of the electroactive tissues (0.4 - 0.9 S/m). Orangi *et al.* dispersed $\text{Ti}_3\text{C}_2\text{Tx}$ MXene and super absorbent polymer beads with DI water and 3D-printed micro-supercapacitors^[73]. The ink showed shear-thinning behavior and the storage modulus larger than the loss modulus ($\tan \delta < 1$), making the ink printable and sustaining the structure without additive at room temperature. The printed structure exhibited outstanding areal capacitances and maximum energy density due to the high electrical conductivity of MXene.

5. Electrode integrated cell culture platform

The extrusion-based printing technology facilitates the embedding of the electrode inside the base polymer

due to its self-healing behavior^[76]. When the electrode is exposed to the surrounding circumstances, it suffers from current leakage, protein fouling, and corrosion, thus reducing the electrode's efficiency and lifecycle^[22,77]. The passivation by encapsulating the electrode prevents direct contact with outer environments, decreasing the threat of damage to the electrode and tissue^[78]. Electrodes can be used either for electrically stimulating the tissues or sensing the electrical properties of tissues. Mature cardiomyocyte shows spontaneous beating behavior and electrical signals related to the calcium ion transient^[79]. Asulin *et al.* fabricated a cardiac patch with built-in electronics that can sense signals and stimulate the tissue at the same time^[71]. The serpentine electrode was printed with PDMS ink with 45 wt% graphite filler that has a conductivity of around 30 S/m. The serpentine structure was selected to reduce the destruction of the electrode by contraction or elongation. The electrode was embedded in PDMS with the surfactant for the hydrophilic property and the cell-laden omentum-based hydrogel surrounds the entire structure. Six electrodes were embedded except for the two ends for the contact and two electrodes were completely exposed to apply an electric field to the engineered tissue. After 7 days of culturing cardiac cells derived from induced pluripotent stem cells, the extracellular potential signals were verified to be similar to those of neonatal ventricular cardiomyocytes. Furthermore, electrical stimulation of 1 or 2 Hz, 7 V, 50 ms-long pulses were applied. The contraction of the engineered tissue synchronized with the electrical stimulation proved the ability to control the tissue.

The electrodes can also be used as strain gauges, as the strain affects the distance between the fillers^[80]. The embedded strain gauge minimizes the reaction with the media and the signal noise. Lind *et al.* printed an embedded strain gauge with TPU ink dispersed with 25 wt% carbon black fillers (CB: TPU)^[72]. The Microgroove PDMS layer was printed above for the biocompatible environment and alignment of cardiomyocytes. The polyamide ink dispersed with silver flake fillers (Ag: PA) was printed afterward for contact between the strain gauge and the wire. As the THF solvent was left inside the CB: TPU ink, the viscosity was dependent on the solvent evaporation and did not show shear-thinning behavior. Meanwhile, Ag: PA ink has $\tan \delta < 1$ at low strain and $\tan \delta > 1$ at high strain, showing high printability and fidelity when stacked. The conductivity of the CB: TPU ink was 84.1 S/m, while the conductivity of the Ag: PA ink was around $1.53 \cdot 10^6$ S/m. As cardiomyocyte matures, the tissue contracts and rolls up the entire platform, leading to the relative resistance change in the strain gauge. The value and the frequency of the relative resistance change

peak was recorded in real-time to analyze the drug's effect on the engineered tissue.

6. Future applications

Electrical stimulation has been adopted as a promising technique for controlling cell behavior. It has been mainly applied to neuronal, cardiac, and muscular tissues that show spontaneous electrical activity. Recently, electrical stimulation has been applied to other tissues, such as skin, and in bone regeneration, accelerating the healing process by elevating cell proliferation and enhancing antimicrobial properties^[81,82]. Furthermore, with increasing studies about the relationship between endocrine cells and the innervation of neurons, the response of pancreatic β -cells to electrical stimulation has been explored^[83]. Various tissue types, signal transduction pathways, and ion transients should be further studied and the electrode integrated cell culture platform can be a major tool for investigating cells' responses.

The versatility of the material and the extrusion-based printing process potentiates the application for complex circuits for drug delivery induced by electrical fields. A drug delivery device is composed of complex circuit connecting sensors, electrical sources, and electrodes^[84]. In addition, removing the need to replace, new batteries during surgery has prompted the conception of wireless designs that transport energy through electromagnetic waves^[85,86]. Sun *et al.*, showed that the 3D circuit design can be directly printed, demonstrating its ability to fabricate intricate circuits^[87]. In summary, 3D printing technology and conductive ink may contribute to the fabrication of a closed-loop drug delivery device that mimics the homeostatic regulation of human body^[84], paving the way for a new generation of therapeutic devices.

Acknowledgments

Not applicable.

Funding

This work was supported by the MSIT (Ministry of Science, ICT), Korea, under the High-Potential Individuals Global Training Program (No. IITP-2021-0-01517) supervised by the IITP (Institute for Information and Communications Technology Planning and Evaluation), and the NRF (National Research Foundation of Korea) grant funded by the Ministry of Science and ICT (MSIT) (No. 2021R1A2C2004981).

Conflict of interest

The authors declare no known conflicts of interest.

Author contributions

Conceptualization: Jihwan Kim, Jinah Jang

Writing - original draft: Jihwan Kim

Writing - review & editing: Jinah Jang

Ethics approval and consent to participate

Not applicable.

Consent for publication

Not applicable.

Availability of data

Not applicable.

References

1. Murphy SV, Atala A, 2014, 3D bioprinting of tissues and organs. *Nat Biotechnol*, 32: 773–785.
<https://doi.org/10.1038/nbt.2958>
2. da Silva LP, Kundu SC, Reis RL, *et al.*, 2020, Electric phenomenon: A disregarded tool in tissue engineering and regenerative medicine. *Trends Biotechnol*, 38: 24–49.
<https://doi.org/10.1016/j.tibtech.2019.07.002>
3. Chen C, Bai X, Ding Y, *et al.*, 2019, Electrical stimulation as a novel tool for regulating cell behavior in tissue engineering. *Biomater Res*, 23: 25.
<https://doi.org/10.1186/s40824-019-0176-8>
4. Yuan X, Arkonac DE, Chao PHG, *et al.*, 2014, Electrical stimulation enhances cell migration and integrative repair in the meniscus. *Sci Rep*, 4: 3674.
<https://doi.org/10.1038/srep03674>
5. Xia Y, Buja LM, Richard CS, *et al.*, 1997, Electrical stimulation of neonatal cardiomyocytes results in the sequential activation of nuclear genes governing mitochondrial proliferation and differentiation. *Proc Natl Acad Sci*, 94: 11399–11404.
<https://doi.org/10.1073/pnas.94.21.11399>
6. Love MR, Palee S, Chattipakorn SC, *et al.*, 2018, Effects of electrical stimulation on cell proliferation and apoptosis. *J Cell Physiol*, 233: 1860–1876.
<https://doi.org/10.1002/jcp.25975>
7. Park D, Park J, Lee J, *et al.*, 2021, Fabrication and characterization of graphene oxide-coated plate for efficient culture of stem cells. *Tissue Eng Regen Med*, 18: 775–785.
<https://doi.org/10.1007/s13770-021-00370-z>
8. Hernández D, Millard R, Sivakumaran P, *et al.*, 2016, Electrical stimulation promotes cardiac differentiation of human induced pluripotent stem cells. *Stem Cells Int*, 2016: 1718041.
<https://doi.org/10.1155/2016/1718041>
9. Hirt MN, Boeddinghaus J, Mitchell A, *et al.*, 2014, Functional improvement and maturation of rat and human engineered heart tissue by chronic electrical stimulation. *J Mol Cell Cardiol*, 74: 151–161.
<https://doi.org/10.1016/j.yjmcc.2014.05.009>
10. LaBarge W, Mattappally S, Kannappan R, *et al.*, 2019, Maturation of three-dimensional, hiPSC-derived cardiomyocyte spheroids utilizing cyclic, uniaxial stretch and electrical stimulation. *PLoS One*, 14: e0219442.
<https://doi.org/10.1371/journal.pone.0219442>
11. Sadeghian RB, Ebrahimi M, Salehi S, 2018, Electrical stimulation of microengineered skeletal muscle tissue: Effect of stimulus parameters on myotube contractility and maturation. *J Tissue Eng Regen Med*, 12: 912–922.
<https://doi.org/10.1002/term.2502>
12. Tandon N, Cannizzaro C, Chao PH, *et al.*, 2009, Electrical stimulation systems for cardiac tissue engineering. *Nat Protoc*, 4: 155–173.
<https://doi.org/10.1038/nprot.2008.183>
13. Harris AR, 2020, Current perspectives on the safe electrical stimulation of peripheral nerves with platinum electrodes. *Bioelectron Med*, 3: 37–49.
<https://doi.org/10.2217/bem-2020-0007>
14. Brummer SB, Turner MJ, 1977, Electrochemical considerations for safe electrical stimulation of the nervous system with platinum electrodes. *IEEE Trans Biomed Eng*, 24: 59–63.
<https://doi.org/10.1109/TBME.1977.326218>
15. Khaw JS, Xue R, Cassidy NJ, *et al.*, 2022, Electrical stimulation of titanium to promote stem cell orientation, elongation and osteogenesis. *Acta Biomater*, 139: 204–217.
<https://doi.org/10.1016/j.actbio.2021.08.010>
16. Shepherd RK, Carter PM, Dalrymple AN, *et al.*, 2021, Platinum dissolution and tissue response following long-term electrical stimulation at high charge densities. *J Neural Eng*, 18: 036021.
<https://doi.org/10.1088/1741-2552/abe5ba>
17. Harnack D, Winter C, Meissner W, *et al.*, 2004, The effects of electrode material, charge density and stimulation duration on the safety of high-frequency stimulation of the subthalamic nucleus in rats. *J Neurosci Methods*, 138: 207–216.
<https://doi.org/10.1016/j.jneumeth.2004.04.019>
18. Ngo TD, Kashani A, Imbalzano G, *et al.*, 2018, Additive manufacturing (3D Printing): A review of materials, methods, applications and challenges. *Compos Part B Eng*, 143: 172–196.
<https://doi.org/10.1016/j.compositesb.2018.02.012>

19. Ravanbakhsh H, Bao G, Luo Z, *et al.*, 2021, Composite inks for extrusion printing of biological and biomedical constructs. *ACS Biomater Sci Eng*, 7: 4009–4026.
<https://doi.org/10.1021/acsbiomaterials.0c01158>
20. Guimarães CF, Gasperini L, Marques AP, *et al.*, 2020, The Stiffness of living tissues and its implications for tissue engineering. *Nat Rev Mater*, 5: 351–370.
<https://doi.org/10.1038/s41578-019-0169-1>
21. Sun X, Sun H, Li H, *et al.*, 2013, Developing polymer composite materials: Carbon nanotubes or graphene? *Adv Mater*, 25: 5153–5176.
<https://doi.org/10.1002/adma.201301926>
22. Schiavone G, Kang X, Fallegger F, *et al.*, 2020, Guidelines to study and develop soft electrode systems for neural stimulation. *Neuron*, 108: 238–258.
<https://doi.org/10.1016/j.neuron.2020.10.010>
23. Chen FM, Liu X, 2016, Advancing biomaterials of human origin for tissue engineering. *Prog Polym Sci*, 53: 86–168.
<https://doi.org/10.1016/j.progpolymsci.2015.02.004>
24. Christopherson GT, de Vasconcellos JF, Dunn JC, *et al.*, 2021, Three-dimensional modeling of the structural microenvironment in post-traumatic war wounds. *Tissue Eng Regen Med*, 18: 963–973.
<https://doi.org/10.1007/s13770-021-00355-y>
25. Skylar-Scott MA, Mueller J, Visser CW, *et al.*, 2019, Voxellated soft matter via multimaterial multinozzle 3D printing. *Nature*, 575: 330–335.
<https://doi.org/10.1038/s41586-019-1736-8>
26. Gillispie G, Prim P, Copus J, *et al.*, 2020, Assessment methodologies for extrusion-based bioink printability. *Biofabrication*, 12: 022003.
<https://doi.org/10.1088/1758-5090/ab6f0d>
27. Franco JM, Partal P, 2010, The newtonian fluid. *Rheology*, 1: 74–95.
28. Viswanath DS, Ghosh TK, Prasad DH, *et al.*, 2007, Viscosity of liquids: theory, estimation, experiment, and data. Berlin, germany: Springer science and business media.
29. Cooke ME, Rosenzweig DH, 2021, The rheology of direct and suspended extrusion bioprinting. *APL Bioeng*, 5: 011502.
<https://doi.org/10.1063/5.0031475>
30. Ferry JD, 1980, Viscoelastic properties of polymers. Hoboken, new jersey: John Wiley and Sons.
31. Mewis J, Wagner NJ, 2009, Thixotropy. *Adv Colloid Interface Sci*, 147–148: 214–227.
<https://doi.org/10.1016/j.cis.2008.09.005>
32. Huang YY, Terentjev EM, 2012, Dispersion of carbon nanotubes: Mixing, sonication, stabilization, and composite properties. *Polymers*, 4: 275–295.
33. Lewis JA, 2000, Colloidal processing of ceramics. *J Am Ceram Soc*, 83:2341–59.
<https://doi.org/10.1111/j.1151-2916.2000.tb01560.x>
34. Ma PC, Siddiqui NA, Marom G, *et al.*, 2010, Dispersion and functionalization of carbon nanotubes for polymer-based nanocomposites: a review. *Compos Part A: Appl Sci Manuf*, 41: 1345–1367.
<https://doi.org/10.1016/j.compositesa.2010.07.003>
35. Li MC, Wu Q, Moon RJ, *et al.*, 2021, Rheological aspects of cellulose nanomaterials: Governing factors and emerging applications. *Adv Mater*, 33: 2006052.
<https://doi.org/10.1002/adma.202006052>
36. Genovese DB, 2012, Shear rheology of hard-sphere, dispersed, and aggregated suspensions, and filler-matrix composites. *Adv Colloid Interface Sci*, 171–2: 1–16.
<https://doi.org/10.1016/j.cis.2011.12.005>
37. Rueda MM, Auscher MC, Fulchiron R, *et al.*, 2017, Rheology and applications of highly filled polymers: A review of current understanding. *Prog Polym Sci*, 66: 22–53.
<https://doi.org/10.1016/j.progpolymsci.2016.12.007>
38. O' Mahony C, Haq EU, Silien C, *et al.*, 2019, Rheological issues in carbon-based inks for additive manufacturing. *Micromachines (Basel)*, 10: 99.
<https://doi.org/10.3390/mi10020099>
39. Fonseca FC, Muccillo R, de Florio DZ, *et al.*, 2007, Mixed ionic-electronic conductivity in yttria-stabilized zirconia/carbon nanotube composites. *Appl Phys Lett*, 91: 243107.
<https://doi.org/10.1063/1.2821373>
40. Mohd Radzuan NA, Sulong AB, Sahari J, 2017, A review of electrical conductivity models for conductive polymer composite. *Int J Hydrogen Energy*, 42: 9262–9273.
<https://doi.org/10.1016/j.ijhydene.2016.03.045>
41. Li C, Thostenson ET, Chou TW, 2007, Dominant role of tunneling resistance in the electrical conductivity of carbon nanotube-based composites. *Appl Phys Lett*, 91: 223114.
<https://doi.org/10.1063/1.2819690>
42. Berhan L, Sastry AM, 2007, Modeling Percolation in High-Aspect-Ratio Fiber Systems. I. Soft-Core Versus Hard-Core Models. *Phys Rev E*, 75:041120.
<https://doi.org/10.1103/PhysRevE.75.041120>
43. Bauhofer W, Kovacs JZ, 2009, A review and analysis of electrical percolation in carbon nanotube polymer composites. *Compos Sci Technol*, 69: 1486–1498.
<https://doi.org/10.1016/j.compscitech.2008.06.018>
44. Leblanc JL, 2002, Rubber-filler interactions and rheological

- properties in filled compounds. *Prog Polym Sci*, 27: 627–687.
[https://doi.org/10.1016/S0079-6700\(01\)00040-5](https://doi.org/10.1016/S0079-6700(01)00040-5)
45. Ravanbakhsh H, Bao G, Latifi N, *et al.*, 2019, Carbon nanotube composite hydrogels for vocal fold tissue engineering: biocompatibility, rheology, and porosity. *Mater Sci Eng C*, 103: 109861.
<https://doi.org/10.1016/j.msec.2019.109861>
46. Islam RR, Md. Hasan A, Md. Abu J, *et al.*, 2019, Carbon nanotubes agglomeration in reinforced composites: A review. *AIMS Mater Sci*, 6: 756–780.
<https://doi.org/10.3934/matserci.2019.5.756>
47. Mora A, Verma P, Kumar S, 2020, Electrical conductivity of cnt/polymer composites: 3D printing, measurements and modeling. *Compos Part B Eng*, 183: 107600.
<https://doi.org/10.1016/j.compositesb.2019.107600>
48. Gong S, Zhu ZH, Li J, *et al.*, 2014, Modeling and characterization of carbon nanotube agglomeration effect on electrical conductivity of carbon nanotube polymer composites. *J Appl Phys*, 116: 194306.
<https://doi.org/10.1063/1.4902175>
49. Liu CX, Choi JW, 2012, Improved dispersion of carbon nanotubes in polymers at high concentrations. *Nanomaterials*, 2: 329–347.
50. Zhu K, Shin SR, van Kempen T, *et al.*, 2017, Gold nanocomposite bioink for printing 3D cardiac constructs. *Adv Funct Mater*, 27: 1605352.
<https://doi.org/10.1002/adfm.201605352>
51. Sahoo NG, Rana S, Cho JW, *et al.*, 2010, Polymer nanocomposites based on functionalized carbon nanotubes. *Prog Polym Sci*, 35: 837–867.
<https://doi.org/10.1016/j.progpolymsci.2010.03.002>
52. Pidcock GC, in het Panhuis M, 2012, Extrusion printing of flexible electrically conducting carbon nanotube networks. *Adv Funct Mater*, 22: 4790–4800.
<https://doi.org/10.1002/adfm.201200724>
53. Punetha VD, Rana S, Yoo HJ, *et al.*, 2017, Functionalization of carbon nanomaterials for advanced polymer nanocomposites: a comparison study between cnt and graphene. *Prog Polym Sci*, 67: 1–47.
<https://doi.org/10.1016/j.progpolymsci.2016.12.010>
54. Ravanbakhsh H, Bao G, Mongeau L, 2020, Carbon nanotubes promote cell migration in hydrogels. *Sci Rep*, 10: 2543.
<https://doi.org/10.1038/s41598-020-59463-9>
55. Jung I, Jo YH, Kim I, *et al.*, 2012, A simple process for synthesis of ag nanoparticles and sintering of conductive ink for use in printed electronics. *J Electron Mater*, 41: 115–21.
<https://doi.org/10.1007/s11664-011-1761-3>
56. Li Y, Pavanram P, Zhou J, *et al.*, 2020, Additively manufactured biodegradable porous zinc. *Acta Biomater*, 101: 609–23.
<https://doi.org/10.1016/j.actbio.2019.10.034>
57. Ahn BY, Duoss EB, Motala MJ, *et al.*, 2009, Omnidirectional printing of flexible, stretchable, and spanning silver microelectrodes. *Science*, 323: 1590–1593.
<https://doi.org/10.1126/science.1168375>
58. Britton J, Krukiewicz K, Chandran M, *et al.*, 2021, A flexible strain-responsive sensor fabricated from a biocompatible electronic ink via an additive-manufacturing process. *Mater Des*, 206: 109700.
<https://doi.org/10.1016/j.matdes.2021.109700>
59. Farizhandi AA, Khalajabadi SZ, Krishnadoss V, *et al.*, 2020, Synthesized biocompatible and conductive ink for 3D printing of flexible electronics. *J Mech Behav Biomed Mater*, 110: 103960.
<https://doi.org/10.1016/j.jmbbm.2020.103960>
60. Doh J, Lee J, 2016, Prediction of the mechanical behavior of double walled-cnts using a molecular mechanics-based finite element method: effects of chirality. *Comput Struct*, 169: 91–100.
<https://doi.org/10.1016/j.compstruc.2016.03.006>
61. Doh J, Park SI, Yang Q, *et al.*, 2019, The effect of carbon nanotube chirality on the electrical conductivity of polymer nanocomposites considering tunneling resistance. *Nanotechnology*, 30: 465701.
<https://doi.org/10.1088/1361-6528/ab3b79>
62. Giavasis I, Harvey LM, McNeil B, 2000, Gellan gum. *Crit Rev Biotechnol*, 20: 177–211.
<https://doi.org/10.1080/07388550008984169>
63. Pedrotty DM, Kuzmenko V, Karabulut E, *et al.*, 2019, Three-dimensional printed biopatches with conductive ink facilitate cardiac conduction when applied to disrupted myocardium. *Circ Arrhythm Electrophysiol*, 12: e006920.
<https://doi.org/10.1161/CIRCEP.118.006920>
64. Jakus AE, Secor EB, Rutz AL, *et al.*, 2015, Three-dimensional printing of high-content graphene scaffolds for electronic and biomedical applications. *ACS Nano*, 9: 4636–4648.
<https://doi.org/10.1021/acsnano.5b01179>
65. García-Tuñón E, Feilden E, Zheng H, *et al.*, 2017, Graphene oxide: an all-in-one processing additive for 3D printing. *ACS Appl Mater Interfaces*, 9: 32977–32989.
<https://doi.org/10.1021/acsmi.7b07717>
66. Shi G, Lowe SE, Teo AJ, *et al.*, 2019, A versatile PDMS submicrobead/graphene oxide nanocomposite ink for the direct ink writing of wearable micron-scale tactile sensors.

- Appl Mater Today*, 16: 482–492.
<https://doi.org/10.1016/j.apmt.2019.06.016>
67. Boularaoui S, Shanti A, Lanotte M, *et al.*, 2021, Nanocomposite conductive bioinks based on low-concentration GelMA and mxene nanosheets/gold nanoparticles providing enhanced printability of functional skeletal muscle tissues. *ACS Biomater Sci Eng*, 7: 5810–5822.
<https://doi.org/10.1021/acsbiomaterials.1c01193>
68. Shin SR, Farzad R, Tamayol A, *et al.*, 2016, A bioactive carbon nanotube-based ink for printing 2D and 3D flexible electronics. *Adv Mater*, 28: 3280–3289.
<https://doi.org/10.1002/adma.201506420>
69. Bordoni M, Karabulut E, Kuzmenko V, *et al.*, 2020, 3D printed conductive nanocellulose scaffolds for the differentiation of human neuroblastoma cells. *Cells*, 9: 682.
<https://doi.org/10.3390/cells9030682>
70. Park J, Jeon N, Lee S, *et al.*, 2022, Conductive hydrogel constructs with three-dimensionally connected graphene networks for biomedical applications. *Chem Eng J*, 446: 137344.
<https://doi.org/10.1016/j.cej.2022.137344>
71. Asulin M, Michael I, Shapira A, *et al.*, 2021, One-step 3D printing of heart patches with built-in electronics for performance regulation. *Adv Sci*, 8: 2004205.
<https://doi.org/10.1002/advs.202004205>
72. Lind JU, Busbee TA, Valentine AD, *et al.*, 2017, Instrumented cardiac microphysiological devices via multimaterial three-dimensional printing. *Nat Mater*, 16: 303–308.
<https://doi.org/10.1038/nmat4782>
73. Orangi J, Hamade F, Davis VA, *et al.*, 2020, 3D printing of additive-free 2D Ti₃C₂T_x (MXene) ink for fabrication of micro-supercapacitors with ultra-high energy densities. *ACS Nano*, 14: 640–650.
<https://doi.org/10.1021/acsnano.9b07325>
74. Naguib M, Mochalin VN, Barsoum MW, *et al.*, 2014, 25th anniversary article: MXenes: A new family of two-dimensional materials. *Adv Mater*, 26: 992–1005.
<https://doi.org/10.1002/adma.201304138>
75. Nasrallah GK, Al-Asmakh M, Rasool K, *et al.*, 2018, Ecotoxicological assessment of Ti₃C₂T_x (MXene) using a zebrafish embryo model. *Environ Sci Nano*, 5: 1002–1011.
<https://doi.org/10.1039/C7EN01239J>
76. Muth JT, Vogt DM, Truby RL, *et al.*, 2014, Embedded 3D printing of strain sensors within highly stretchable elastomers. *Adv Mater*, 26: 6307–6312.
<https://doi.org/10.1002/adma.201400334>
77. Merrill DR, 2010, The electrochemistry of charge injection at the electrode/tissue interface. In: Zhou d, greenbaum e, editors. *Implantable neural prostheses 2: Techniques and engineering approaches*. New York: Springer. p85–p138.
78. Merrill DR, Bikson M, Jefferys JG, 2005, Electrical stimulation of excitable tissue: Design of efficacious and safe protocols. *J Neurosci Methods*, 141: 171–198.
<https://doi.org/10.1016/j.jneumeth.2004.10.020>
79. Nunes SS, Miklas JW, Liu J, *et al.*, 2013, Biowire: A platform for maturation of human pluripotent stem cell-derived cardiomyocytes. *Nat Methods*, 10: 781–787.
<https://doi.org/10.1038/nmeth.2524>
80. Shakeel M, Khan WA, Rahman K, 2017, Fabrication of cost effective and high sensitivity resistive strain gauge using diw technique. *Sens Actuators A Phys*, 258: 123–130.
<https://doi.org/10.1016/j.sna.2017.03.003>
81. Leppik L, Oliveira KM, Bhavsar MB, *et al.*, 2020, Electrical stimulation in bone tissue engineering treatments. *Eur J Trauma Emerg Surg*, 46: 231–244.
<https://doi.org/10.1007/s00068-020-01324-1>
82. Talikowska M, Fu X, Lisak G, 2019, Application of conducting polymers to wound care and skin tissue engineering: A review. *Biosens Bioelectron*, 135: 50–63.
<https://doi.org/10.1016/j.bios.2019.04.001>
83. Liebman C, Vu TM, Phillips A, *et al.*, 2021, Altered β -cell calcium dynamics via electric field exposure. *Ann Biomed Eng*, 49: 106–114.
<https://doi.org/10.1007/s10439-020-02517-w>
84. Yu J, Zhang Y, Yan J, *et al.*, 2018, Advances in bioresponsive closed-loop drug delivery systems. *Int J Pharm*, 544: 350–357.
<https://doi.org/10.1016/j.ijpharm.2017.11.064>
85. Tetsuka H, Pirrami L, Wang T, *et al.*, 2022, Wirelessly powered 3D printed hierarchical biohybrid robots with multiscale mechanical properties. *Adv Funct Mater*, 32: 2202674.
<https://doi.org/10.1002/adfm.202202674>
86. Mirvakili SM, Langer R, 2021, Wireless on-demand drug delivery. *Nat Electron*, 4:464–77.
<https://doi.org/10.1038/s41928-021-00614-9>
87. Sun P, Zhang J, Zhu X, *et al.*, Directly printed interconnection wires between layers for 3D integrated stretchable electronics. *Adv Mater Technol*, 7: 2200302.
<https://doi.org/10.1002/admt.202200302>